Nuclear Science and Techniques (2025) 36:222
https://doi.org/10.1007/s41365-025-01812-2

Ab initio calculations of the highest-multipole electromagnetic transition ever observed in nuclei

Si-Qin Fan[1] · Qi Yuan[1,2] · Fu-Rong Xu[1,2,3] · Philip Malzard Walker[3]

Received: 24 April 2025 / Revised: 4 June 2025 / Accepted: 19 June 2025 / Published online: 12 September 2025

Abstract
High multipole electromagnetic transitions are rare in nature. The highest-multipole transition observed in atomic nuclei is the electric hexacontatetrapole $E6$ transition from the $T_{1/2} = 2.54(2)$-min $J^\pi = 19/2^-$ isomer to the $7/2^-$ ground state in ^{53}Fe with an angular momentum change of six units. In the present work, we performed ab initio calculations for this unique case by employing chiral effective field theory (EFT) forces. The in-medium similarity renormalization group is used to derive the valence-space effective Hamiltonian and multipolar transition operators. Bare nucleon charges were used in all the multipolar transition rate calculations, providing good agreement with the experimental data. The valence space takes the full fp shell. In ^{53}Fe, the low-lying states were dominated by the $0f_{7/2}$ component. Two different versions of the chiral EFT two- plus three-nucleon interaction were used to test the dependence on the interaction used. We also tested the convergence of the transition rate calculations against the harmonic oscillator parameter $\hbar\Omega$ and basis truncations $e_{\max}$ and $E_{3\max}$ for two- and three-nucleon forces, respectively.

Keywords Isomerism · Highest-multipole electromagnetic transitions · Ab initio calculations · Chiral two- plus three-nucleon forces · Valence-space in-medium similarity renormalization group

1 Introduction

The $T_{1/2} = 2.54$-min $J^\pi = 19/2^-$ isomer at 3.0 MeV in ^{53}Fe is unique in atomic nuclei in that it has a direct decay branch to the $J^\pi = 7/2^-$ ground state, requiring a hexacontatetrapole electric transition $E6$ [1–3]. This was recently experimentally confirmed with improved precision [4], providing a sensitive probe for nuclear structures [5, 6]. More generally, this scenario provides unique insights into the highest order shapes and correlations in nuclei, and tests the applicability of nuclear models under extreme conditions. In the present work, we focus on ab initio calculations with bare nucleon charges, which can explain both ^{53}Fe excited-state energies and electromagnetic decay transition rates.

In nature, a free photon has an angular momentum of $1\hbar$, whereas in a high multipole transition, a single photon carries away a large angular momentum. Naively, the probability of emitting a high-spin photon should be very small. In ^{53}Fe, a single $E6$ photon brings a spin change as large as $6\hbar$. No other isolated physical system is known to exhibit high multipole or single-photon emission. By comparison, infrared spectra have revealed $6\hbar$ absorption in solid hydrogen [7], and magneto-optical studies of atomic ^{85}Rb have reported $6\hbar$ spontaneous emissions [8]. Thus, there is a small group of physical environments where high multipole radiation provides access to novel and exceptional physics.

In a recent experimental study by Palazzo et al. [4], the existence of $E6$ decay in ^{53}Fe was firmly established using empirical shell model calculations. However, Ref. [4] does

This work was supported by the National Key R&D Program of China (Nos. 2024YFA1610900 and 2023YFA1606401), the National Natural Science Foundation of China (Nos. 12335007 and 12035001), and the United Kingdom Science and Technology Facilities Council (No. ST/V001108/1).

✉ Fu-Rong Xu
frxu@pku.edu.cn

[1] School of Physics, and State Key Laboratory of Nuclear Physics and Technology, Peking University, Beijing 100871, China

[2] Southern Center for Nuclear-Science Theory (SCNT), Institute of Modern Physics, Huizhou 516000, China

[3] Department of Physics, University of Surrey, Guildford GU2 7XH, UK

not provide calculations of high multipole electromagnetic transition probabilities. This is because that the empirical calculations require both proton and neutron effective charges that cannot be determined at present by only one available set of experimental $E6$ transition rate data. In empirical models, different effective charges are used for different multipolarities of the transitions. To improve such *ad hoc* features, ab initio calculations that use realistic interactions and bare nucleon charges are required. This provides the prospect of gaining insight into rare high-multipole transitions and testing the ab initio method itself. The ab initio nuclear theory is at the forefront of the current nuclear structure studies. Over the past two decades, significant progress has been made in ab initio many-body methods [9–13] using nuclear forces based on chiral effective field theory [14].

In this study, we employed the ab initio valence-space in-medium similarity renormalization group (VS-IMSRG) [15–18] to derive the valence-space effective Hamiltonian and effective multipole transition operators for further shell model calculations of the observed excited states and their electromagnetic transitions in ^{53}Fe. Unique bare nucleon charges were used in the calculation of all the multipolar transitions. We aim to provide solid calculations to explain the experimental observations and provide deep insight into the structure of the $J^\pi = 19/2^-$ isomer.

2 Theoretical framework

Our calculations start from the intrinsic Hamiltonian of the A-nucleon system [19, 20]

$$H = \sum_{i=1}^{A}\left(1-\frac{1}{A}\right)\frac{\boldsymbol{p}_i^2}{2m} + \sum_{i<j}^{A}\left(v_{ij}^{\mathrm{NN}} - \frac{\boldsymbol{p}_i\cdot\boldsymbol{p}_j}{mA}\right) + \sum_{i<j<k}^{A} v_{ijk}^{\mathrm{3N}}, \tag{1}$$

where $\boldsymbol{p}_i$ is the nucleon momentum in the laboratory system, m is the nucleon mass, and v_{ij}^{NN} and v_{ijk}^{3N} represent the nucleon-nucleon (NN) and three-nucleon (3N) interactions, respectively. An explicit treatment of the three-nucleon force (3NF) in many-body calculations has not yet been accessible for nuclei as heavy as ^{53}Fe. Therefore, we obtain a normal-ordered approximation of the Hamiltonian (Eq. (1), neglecting the residual 3NF [20–24].

The IMSRG evolves the normal-ordered Hamiltonian to a block diagonal, which gives the valence-space effective Hamiltonian. Using this technique, we can also derive valence-space effective operators for other observables, including multipolar transitions. The Magnus expansion [25] was used in the IMSRG evolution. Operators appearing in the IMSRG equations are truncated at the two-body level, which is referred to as IMSRG(2) [21].

The technique of using IMSRG to obtain a valence-space Hamiltonian for shell model calculations is called VS-IMSRG [21].

The normal-ordering approximation of the Hamiltonian and the evolution of the VS-IMSRG were implemented with a closed-shell reference state in the Hartree-Fock basis. However, to reduce the effect of the residual 3NF, which is neglected, the fractional filling of open-shell orbitals in an open-shell nucleus has been suggested, called ensemble normal ordering (ENO) [17]. Using the ENO approximation of the VS-IMSRG, we can obtain the nucleus-dependent valence-space effective Hamiltonian and the effective operators of the other observables. The effective Hamiltonian obtained is diagonalized using the large-scale shell model code KSHELL [26], giving eigenenergies and one- and two-body transition densities (OBTD and TBTD, respectively) for further calculations of states.

The reduced transition probability is calculated by

$$B(\sigma\lambda;\psi_i\to\psi_f) = \frac{|\langle\psi_f\|\boldsymbol{\mathcal{M}}_{\sigma\lambda}\|\psi_i\rangle|^2}{2J_i+1}, \tag{2}$$

where σ denotes the electric ($\sigma = E$) or magnetic ($\sigma = M$) transition and λ is the rank of the tensor operator $\mathcal{M}_{\sigma\lambda}$ [27]. $\psi_i(\psi_f)$ represents the initial (final) state of the transition, where J_i denotes the angular momentum of the initial state. The free-space bare electric transition tensor operator is defined by $\boldsymbol{\mathcal{M}}_{E\lambda} = \boldsymbol{Q}_\lambda$ with the tensor components given by [28]

$$Q_{\lambda\mu} = \sum_{j=1}^{A} e_j r_j^\lambda Y_{\lambda\mu}(\hat{r}_j), \tag{3}$$

where e_j is the natural (bare) charge of the jth nucleon, that is, $e = 1$ (0) for the proton (neutron). $Y_{\lambda\mu}$ is the spherical harmonic function. The free-space bare magnetic transition tensor operator is defined by $\boldsymbol{\mathcal{M}}_{M\lambda} = \boldsymbol{M}_\lambda$ with the tensor components given by [28]

$$M_{\lambda\mu} = \sum_{j=1}^{A}\left[\frac{2}{\lambda+1}g_l^j\boldsymbol{l}_j + g_s^j\boldsymbol{s}_j\right]\cdot\nabla_j\left[r_j^\lambda Y_{\lambda\mu}(\hat{r}_j)\right], \tag{4}$$

where $\boldsymbol{l}_j$ and $\boldsymbol{s}_j$ are the orbital and intrinsic angular momenta of the jth nucleon, respectively. The values of g factors were taken from [28]. The free-space bare operators, $\boldsymbol{\mathcal{M}}_{\sigma\lambda}$, must be renormalized into the valence space, which can be performed using the same ENO VS-IMSRG technique. After renormalization, the one-body operators of the free space bare $\boldsymbol{\mathcal{M}}_{\sigma\lambda}$ become two-body operators in the valence space, defined by the corresponding two-body matrix elements. Using the valence-space OBTD and TBTD obtained in the diagonalization of the effective Hamiltonian, the reduced transition probability is calculated using Eq. (2).

3 Calculations and discussions

The ^{53}Fe $J^\pi = 19/2^-$ isomer is the only case in which the highest-multipole $E6$ transition is observed [1–4]. In a recent experimental study [4], shell model calculations using two empirical interactions, GFPX1A and KB3G, were performed with a model space of only the $0f_{7/2}$ or the full fp shell. In empirical calculations of electromagnetic transitions, effective nucleon charges are used with different effective charges for different multipolarities of transitions, determined by fitting the data. The problem is that only one $E6$ transition has been observed to date, that is, from the $19/2^-$ isomer to the $7/2^-$ ground state in ^{53}Fe. One $E6$ transition data cannot simultaneously determine both the proton and neutron effective charges. In the present work, we performed ab initio calculations using the shell model with a full fp model space above the ^{40}Ca core. The valence-space shell model effective Hamiltonian, including the one-body single-particle energies of the valence particles, is obtained using the IMSRG evolution with the ENO approximation [17, 21]. In ab initio calculations of multipole transitions, unique bare nucleon charges are used, meaning that the same bare charges are used for different multipolarities of the transitions.

In our calculations, two different versions of the chiral NN plus 3N interaction were used to test its dependence on the interaction used. The potential labeled 1.8/2.0(EM) [29–31] takes the NN force (2NF) at N^{3}LO [32] and 3NF at N^{2}LO. This potential can globally reproduce the ground-state properties of nuclei, from light-to heavy-mass regions, with the harmonic-oscillator (HO) basis frequency optimized at $\hbar\Omega = 16$ MeV [33, 34]. We also used the recently developed interaction labeled by NN+3N(lnl) [35, 36] in which N^{4}LO 2NF and N^{2}LO 3NF were used. For both the 1.8/2.0(EM) and NN+3N(lnl) potentials, the induced 3NF was properly included [29–31, 35, 36]. One major difference between the two potentials was the treatment with 3NF. The 1.8/2.0(EM) potential uses a nonlocal 3N regulator, whereas the NN+3N(lnl) potential employs both local and nonlocal (lnl) 3N regulators.

The basis space is another important issue that must be addressed. The present calculation starts by using a spherical HO basis with $e = 2n + l \le e_{\max}$ single-particle shells. The 3NF is limited to $e_1 + e_2 + e_3 \le E_{3\max}$. For the 1.8/2.0(EM) and NN+3N(lnl) potentials, it has been demonstrated that basis truncations with both $e_{\max}$ and $E_{3\max}$ around 14 can provide good convergence of VS-IMSRG calculations, particularly for ground-state energies up to medium-mass regions, with an optimized frequency around $\hbar\Omega = 16$ MeV [31, 33, 35, 36]. However, spectroscopic calculations of heavier nuclei would require larger basis space. For example, a recent study using the 1.8/2.0(EM) potential showed that $E_{3\max} = 24$ is required to achieve convergence of the calculations of excited states in $A \approx 130$ mass region [34]. Another study on the neutrinoless double-beta decay ($0\nu\beta\beta$) of $A \approx 130$ candidates showed that $E_{3\max} = 28$ is required to converge all the operators [37]. However, both studies show that $e_{\max} = 14$ is sufficient for truncation of the single-particle basis. In the present work, we tested the convergence of the calculations of the observed highest-multipole electromagnetic transition probabilities for which no ab initio calculations have been performed previously. Figure 1 shows the convergence of the $E4$, $M5$ and $E6$ reduced transition probabilities as a function of $e_{\max}$, $E_{3\max}$ and $\hbar\Omega$. We observe that at both potentials, the calculations converge well at $e_{\max} \ge 12$, $E_{3\max} \ge 16$ and $\hbar\Omega = 14 - 16$ MeV. Therefore, in the following calculations, we consider $e_{\max} = 14$, $E_{3\max} = 24$, and $\hbar\Omega = 16$ MeV. This choice is similar to that used in the calculations of the excitation spectra [34] and $0\nu\beta\beta$ decays [37] in the mass 130 region.

The present calculations reproduce the excitation spectrum of ^{53}Fe. However, for the sake of simplicity, as shown in Fig. 2 we show only a limited set of levels associated with the $19/2^-$ isomer. The calculations reproduced experimental data [38]. In particular, the calculation using the NN+3N(lnl) interaction was in better agreement with the data. Both calculations yield the correct energy ordering of the $19/2^-$ level, which is lower than the $13/2^-$ level. The lower energy of the $19/2^-$ level compared to that of the $17/2^-$ and $15/2^-$ levels makes it natural that the $M1$ and $E2$ transitions cannot occur from the $19/2^-$ state, which leads to the formation of the $19/2^-$ metastable isomeric state.

Experiments [1–4] observed that the $19/2^-$ states decayed to lower $11/2^-$, $9/2^-$ and $7/2^-$ states by high-multipole $E4$,

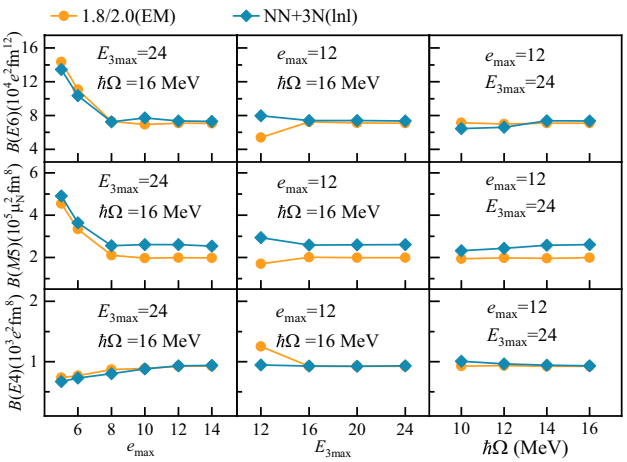

Fig. 1 Calculated reduced probabilities of the $E6$, $M5$ and $E4$ transitions from the $19/2^-$ isomer in ^{53}Fe, as functions of $e_{\max}$, $E_{3\max}$ and $\hbar\Omega$. The 1.8/2.0(EM) and NN+3N(lnl) potentials were used

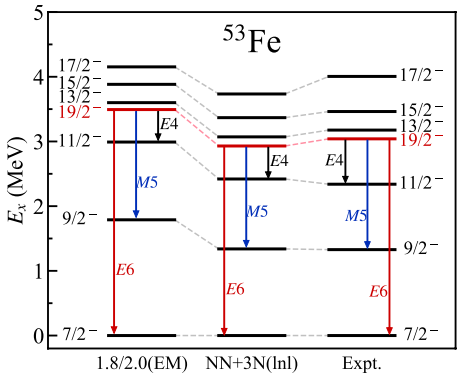

Fig. 2 Calculated levels involved in the observed highest-multipole $E6$, $M5$ and $E4$ electromagnetic transitions from the $19/2^-$ isomer in ^{53}Fe, compared with data [38]. The 1.8/2.0(EM) and NN+3N(lnl) potentials were used

Table 1 Calculated reduced probabilities $B(\sigma\lambda)$ of the highest-multipole $E6$, $M5$ and $E4$ transitions from the $19/2^-$ isomer observed in ^{53}Fe. $B(\sigma\lambda)$ is shown in units of $e^2fm^{2\lambda}$ for the 2^λ-pole electric transition, and $\mu_N^2 fm^{2\lambda-2}$ for the 2^λ-pole magnetic transition. The 1.8/2.0(EM) and NN+3N(lnl) potentials are used. The experimental data are taken from Ref. [4]

Transitions	$\sigma\lambda$	$B(\sigma\lambda)\left(e^2fm^{2\lambda}/\mu_N^2 fm^{2\lambda-2}\right)$		
		1.8/2.0(EM)	NN+3N(lnl)	Expt.
$19/2^- \to 7/2^-$	$E6$	0.706×10^5	0.725×10^5	$2.61(81)\times10^5$
$19/2^- \to 9/2^-$	$M5$	1.98×10^5	2.53×10^5	$3.31(16)\times10^5$
$19/2^- \to 11/2^-$	$E4$	9.28×10^2	9.58×10^2	$6.46(5)\times10^2$

$M5$ and $E6$ transitions, respectively. Higher multipole γ decays have lower transition probabilities, which can lead to long-lived isomers. Experimental observations [1–4] of the rare high multipole γ decay in ^{53}Fe provide a unique laboratory for the study of electromagnetic transitions with high multipolarity. Table 1 shows the calculated reduced probabilities of the observed highest-multipole transitions $E6$, $M5$ and $E4$ compared with the experimental data [4]. The NN+3N(lnl) potential provides an improved result for the $M5$ transition probability that is closer to the data. However, the calculated $E6$ transition probability differed from the experimental data by a factor of approximately three, although the experimental error was large for this transition. The present VS-IMSRG calculation is approximated with operators truncated at a two-body level by IMSRG(2) [21], whereas a recent study has developed the IMSRG with operators truncated at the three-body level labeled by IMSRG(3) [39, 40]. Another study indicated that the IMSRG combined with the generator coordinate method can capture more collective correlations in deformed nuclei [41]. In Refs. [42, 43], it was found that the inclusion of two-body currents can improve the calculation of magnetic dipole moments

Table 2 Similar to Table 1, but for $E2$ and $M1$ transitions in ^{53}Fe. Data are from [38]

$\sigma\lambda$	Transitions	$B(\sigma\lambda)\left(e^2fm^{2\lambda}/\mu_N^2 fm^{2\lambda-2}\right)$		
		1.8/2.0(EM)	NN+3N(lnl)	Expt.
$E2$	$11/2^- \to 9/2^-$	108	104	106(47)
	$9/2^- \to 7/2^-$	139	127	94(59)
$M1$	$11/2^- \to 9/2^-$	0.81	0.79	0.63(14)
	$9/2^- \to 7/2^-$	0.51	0.51	0.98(41)

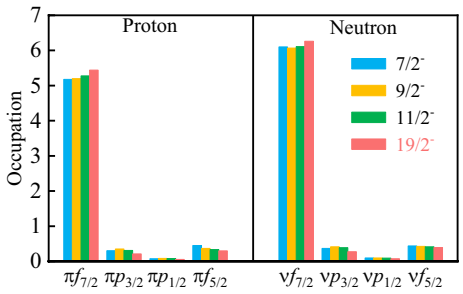

Fig. 3 (Color online) Configurations of the $7/2^-$, $9/2^-$, $11/2^-$, and $19/2^-$ states, obtained in the present calculations with the NN+3N(lnl) interaction

(transitions). It is clear that the consideration of these factors can improve calculations, but such an investigation goes beyond the scope of the present work and will be addressed separately. In empirical shell model calculations, effective nucleon charges are used to compensate for missing correlations. The values of the proton and neutron effective charges were determined by fitting the corresponding experimental data to the electromagnetic transitions. Different effective charges of protons and neutrons are used for different multipolarities of the transitions. Unfortunately, only one $E6$ experimental data point is available at present, which is not sufficient to determine both the proton and neutron effective charges of the $E6$ transition.

Using bare nucleon charges, we also calculated the ^{53}Fe $E2$ and $M1$ reduced transition probabilities that were available experimentally, as shown in Table 2. We observe that the observed $E2$ and $M1$ transition probabilities can be reproduced reasonably well (all are well within 2σ of the experimental values). Nevertheless, improvements in the IMSRG and the inclusion of two-body currents should also improve the calculations of low-multipole transitions.

To better understand the long-lived $19/2^-$ isomer of ^{53}Fe, we discuss the state configurations. Figure 3 shows the configurations of the $7/2^-$, $9/2^-$, $11/2^-$ and $19/2^-$ states obtained from the calculation. We see that the $0f_{7/2}$ component dominates the states, which can be understood by the simple three-hole ($3h$) coupling $(f_{7/2})^{-2}(f_{7/2})^{-1}$ with $J = 19/2$ being the highest spin that can be obtained in $3h$

coupling. As shown in Fig. 3, the $19/2^-$ isomer has a purer $0f_{7/2}$ component, with fewer occupations in the higher $0f_{5/2}$ and $1p_{3/2,1/2}$ orbitals. The pronounced dominance of the $0f_{7/2}$ component for both neutron and proton orbits arises from the $N(Z) = 28$ shell gaps on either side of the $f_{7/2}$ orbit. However, we find that the effects of the higher $0f_{5/2}$ and $1p_{3/2}$ orbitals are not negligible.

4 Summary

High-multipole electromagnetic transitions are of particular interest in the study of nuclear structures, providing a sensitive test of the theories used. To date, the highest-multipole transition is the electric hexacontatetrapole $E6$ transition from the $J^\pi = 19/2^-$ isomer to the $7/2^-$ ground state in ^{53}Fe, accompanied by $M5$ and $E4$ transitions to the first $9/2^-$ and $11/2^-$ excited states, respectively. A recent experiment [4] provided clear detection of the highest-multipole transitions with greater precision for the transition rates. Shell-model calculations with empirical interactions were performed in an experimental study [4]. However, empirical calculations cannot definitively determine the $E6$ transition probability. The empirical shell model uses the effective charges determined by fitting the experimental data. To date, only one $E6$ transition was observed, i.e., that from the $J^\pi = 19/2^-$ isomer to the $J^\pi = 7/2^-$ ground state in ^{53}Fe. An experimental $E6$ transition rate cannot simultaneously determine both the proton and neutron effective charges.

In this study, we performed ab initio calculations of the highest-multipole electromagnetic transitions observed from the $19/2^-$ isomer of ^{53}Fe. Two different versions of the chiral two-plus three-nucleon interactions were used in the calculations. Using the valence-space in-medium similarity renormalization group, the free-space interaction matrix was decoupled to form a low-momentum valence space, obtaining the valence-space effective interaction for the shell-model calculation. The calculation convergence of the excitation spectrum and the electromagnetic transitions of ^{53}Fe has been well tested. The present ab initio calculations reproduce the experimental spectrum well. The $19/2^-$ isomerism is due to its lower energy compared to those of the $17/2^-$ and $15/2^-$ levels, which leads to the absence of natural $E2$ and $M1$ transitions from the $19/2^-$ state. Using the same decoupling method, free-space bare operators of electromagnetic transitions evolve into the valence space. With the unique bare nucleon charges, we can reproduce the measured highest-multipole $E6$, $M5$ and $E4$ transition strengths. The low multipole $E2$ and $M1$ transitions observed in this nucleus can also be reproduced using bare nucleon charges. Moreover, we provide the configurations of the $7/2^-, 9/2^-, 11/2^-$ and $19/2^-$ states, and reveal the structure of the $J^\pi = 19/2^-$ isomer.

Acknowledgements We thank Takayuki Miyagi for the `NuHamil` code [44] used to generate matrix elements of the chiral three-body interaction. We thank Rong Zhe Hu, Bai Shan Hu and Shao Liang Jin for their valuable suggestions and discussions. We acknowledge the High-Performance Computing Platform of Peking University for providing computational resources.

Author contributions All authors contributed to the study conception and design. Material preparation, data collection and analysis were performed by Si-Qin Fan and Qi Yuan. The first draft of the manuscript was written by Si-Qin Fan and all authors commented on previous versions of the manuscript. All authors read and approved the final manuscript.

Data availability The data that support the findings of this study are openly available in Science Data Bank at https://cstr.cn/31253.11.sciencedb.28563 and https://doi.org/10.57760/sciencedb.28563.

Declarations

Conflict of interest Fu-Rong Xu is an editorial board member for Nuclear Science and Techniques and was not involved in the editorial review, or the decision to publish this article. All authors declare that there are no Conflict of interest.

References

1. J.N. Black, W.C. McHarris, W.H. Kelly, *E6* and *M5* transitions observed in Fe ^{53m} decay. Phys. Rev. Lett. **26**, 451–454 (1971). https://doi.org/10.1103/PhysRevLett.26.451
2. J.N. Black, W.C. McHarris, W.H. Kelly et al., Decays of the $f_{\frac{7}{2}}$ isomers ^{53}Fe^g and ^{53}Fe^m. Phys. Rev. C **11**, 939–951 (1975). https://doi.org/10.1103/PhysRevC.11.939
3. D.F. Geesaman, R.L. McGrath, J.W. Noé et al., Yrast states in ^{52}Fe, ^{52}Mn and the decay of ^{52}Fe^m. Phys. Rev. C **19**, 1938–1947 (1979). https://doi.org/10.1103/PhysRevC.19.1938
4. T. Palazzo, A.J. Mitchell, G.J. Lane et al., Direct measurement of hexacontatetrapole, *E6γ* decay from ^{53m}Fe. Phys. Rev. Lett. **130**, 122503 (2023). https://doi.org/10.1103/PhysRevLett.130.122503
5. B.A. Brown, W.D.M. Rae, E6 gamma decay. AIP Conf. Proc. **1355**, 145–152 (2011). https://doi.org/10.1063/1.3584058
6. B.A. Brown, Shell-model description of nuclear isomers. Eur. Phys. J. Special Topics **233**, 893–902 (2024). https://doi.org/10.1140/epjs/s11734-024-01137-y
7. M. Okumura, M.C. Chan, T. Oka, High-resolution infrared spectroscopy of solid hydrogen: the tetrahexacontapole-induced $\Delta J = 6$ transitions. Phys. Rev. Lett. **62**, 32–35 (1989). https://doi.org/10.1103/PhysRevLett.62.32
8. S. Pustelny, D.F. Jackson Kimball, S.M. Rochester et al., Pump-probe nonlinear magneto-optical rotation with frequency-modulated light. Phys. Rev. A **73**, 023817 (2006). https://doi.org/10.1103/PhysRevA.73.023817
9. H. Hergert, A guided tour of *ab initio* nuclear many-body theory. Front. Phys. **8**, 379 (2020). https://doi.org/10.3389/fphy.2020.00379
10. B.S. Hu, W.G. Jiang, T. Miyagi et al., *Ab initio* predictions link the neutron skin of ^{208}Pb to nuclear forces. Nat. Phys. **18**, 1196–1200 (2022). https://doi.org/10.1038/s41567-022-01715-8

11. X.Y. Xu, S.Q. Fan, Q. Yuan et al., Progress in *ab initio* in-medium similarity renormalization group and coupled-channel method with coupling to the continuum. Nucl. Sci. Tech. **35**, 215 (2024). https://doi.org/10.1007/s41365-024-01585-0
12. Y.L. Ye, X.F. Yang, H. Sakurai et al., Physics of exotic nuclei. Nat. Rev. Phys. 7, 21–37 (2025). https://doi.org/10.1038/s42254-024-00782-5
13. J.G. Li, B.S. Hu, S. Zhang et al., Unbound ^{28}O, the heaviest oxygen isotope observed: a cutting-edge probe for testing nuclear models. Nucl. Sci. Tech. **35**, 21 (2024). https://doi.org/10.1007/s41365-024-01373-w
14. R. Machleidt, D. Entem, Chiral effective field theory and nuclear forces. Phys. Rep. **503**, 1–75 (2011). https://doi.org/10.1016/j.physrep.2011.02.001
15. K. Tsukiyama, S.K. Bogner, A. Schwenk, In-medium similarity renormalization group for open-shell nuclei. Phys. Rev. C **85**, 061304(R) (2012). https://doi.org/10.1103/PhysRevC.85.061304
16. H. Hergert, S. Bogner, T. Morris et al., The in-medium similarity renormalization group: a novel *ab initio* method for nuclei. Phys. Rep. **621**, 165 (2016). https://doi.org/10.1016/j.physrep.2015.12.007
17. S.R. Stroberg, A. Calci, H. Hergert et al., Nucleus-dependent valence-space approach to nuclear structure. Phys. Rev. Lett. **118**, 032502 (2017). https://doi.org/10.1103/PhysRevLett.118.032502
18. T. Miyagi, S.R. Stroberg, J.D. Holt et al., *Ab initio* Multishell valence-space Hamiltonians and the island of inversion. Phys. Rev. C **102**, 034320 (2020). https://doi.org/10.1103/PhysRevC.102.034320
19. S. Zhang, Y.Z. Ma, J.G. Li et al., The roles of three-nucleon force and continuum coupling in mirror symmetry breaking of oxygen mass region. Phys. Lett. B **827**, 136958 (2022). https://doi.org/10.1016/j.physletb.2022.136958
20. S. Zhang, F.R. Xu, J.G. Li et al., *Ab initio* descriptions of $A = 16$ mirror nuclei with resonance and continuum coupling. Phys. Rev. C **108**, 064316 (2023). https://doi.org/10.1103/PhysRevC.108.064316
21. K. Tsukiyama, S.K. Bogner, A. Schwenk, In-medium similarity renormalization group for nuclei. Phys. Rev. Lett. **106**, 222502 (2011). https://doi.org/10.1103/PhysRevLett.106.222502
22. Y.Z. Ma, L. Coraggio, L. De Angelis et al., Contribution of chiral three-body forces to the monopole component of the effective shell-model Hamiltonian. Phys. Rev. C **100**, 034324 (2019). https://doi.org/10.1103/PhysRevC.100.034324
23. G. Hagen, T. Papenbrock, D.J. Dean et al., Coupled-cluster theory for three-body Hamiltonians. Phys. Rev. C **76**, 034302 (2007). https://doi.org/10.1103/PhysRevC.76.034302
24. R. Roth, S. Binder, K. Vobig et al., Medium-mass nuclei with normal-ordered chiral *NN*+3*N* interactions. Phys. Rev. Lett. **109**, 052501 (2012). https://doi.org/10.1103/PhysRevLett.109.052501
25. T.D. Morris, N.M. Parzuchowski, S.K. Bogner, Magnus expansion and in-medium similarity renormalization group. Phys. Rev. C **92**, 034331 (2015). https://doi.org/10.1103/PhysRevC.92.034331
26. N. Shimizu, T. Mizusaki, Y. Utsuno et al., Thick-restart block Lanczos method for large-scale shell-model calculations. Comput. Phys. Commun. **244**, 372–384 (2019). https://doi.org/10.1016/j.cpc.2019.06.011
27. N.M. Parzuchowski, S.R. Stroberg, P. Navrátil et al., *Ab initio* electromagnetic observables with the in-medium similarity renormalization group. Phys. Rev. C **96**, 034324 (2017). https://doi.org/10.1103/PhysRevC.96.034324
28. J. Suhonen, From Nucleons to Nucleus. Concepts of Microscopic Nuclear Theory (2013)
29. K. Hebeler, S.K. Bogner, R.J. Furnstahl et al., Improved nuclear matter calculations from chiral low-momentum interactions. Phys. Rev. C **83**, 031301(R) (2011). https://doi.org/10.1103/PhysRevC.83.031301
30. J. Simonis, K. Hebeler, J.D. Holt et al., Exploring *sd*-shell nuclei from two- and three-nucleon interactions with realistic saturation properties. Phys. Rev. C **93**, 011302(R) (2016). https://doi.org/10.1103/PhysRevC.93.011302
31. J. Simonis, S.R. Stroberg, K. Hebeler et al., Saturation with chiral interactions and consequences for finite nuclei. Phys. Rev. C **96**, 014303 (2017). https://doi.org/10.1103/PhysRevC.96.014303
32. D.R. Entem, R. Machleidt, Accurate charge-dependent nucleon-nucleon potential at fourth order of chiral perturbation theory. Phys. Rev. C **68**, 041001 (2003). https://doi.org/10.1103/PhysRevC.68.041001
33. S.R. Stroberg, J.D. Holt, A. Schwenk et al., *Ab initio* limits of atomic nuclei. Phys. Rev. Lett. **126**, 022501 (2021). https://doi.org/10.1103/PhysRevLett.126.022501
34. T. Miyagi, S.R. Stroberg, P. Navrátil et al., Converged *ab initio* calculations of heavy nuclei. Phys. Rev. C **105**, 014302 (2022). https://doi.org/10.1103/PhysRevC.105.014302
35. V. Somà, P. Navrátil, F. Raimondi et al., Novel chiral Hamiltonian and observables in light and medium-mass nuclei. Phys. Rev. C **101**, 014318 (2020). https://doi.org/10.1103/PhysRevC.101.014318
36. P. Gysbers, G. Hagen, J.D. Holt et al., Discrepancy between experimental and theoretical β-decay rates resolved from first principles. Nat. Phys. **15**, 428 (2019). https://doi.org/10.1038/s41567-019-0450-7
37. A. Belley, T. Miyagi, S.R. Stroberg et al., Ab initio calculations of neutrinoless ββ decay refine neutrino mass limits. arXiv: 2307.15156
38. https://www.nndc.bnl.gov/ensdf/
39. M. Heinz, A. Tichai, J. Hoppe et al., In-medium similarity renormalization group with three-body operators. Phys. Rev. C **103**, 044318 (2021). https://doi.org/10.1103/PhysRevC.103.044318
40. S.R. Stroberg, T.D. Morris, B.C. He, In-medium similarity renormalization group with flowing 3-body operators, and approximations thereof. Phys. Rev. C **110**, 044316 (2024). https://doi.org/10.1103/PhysRevC.110.044316
41. J.M. Yao, B. Bally, J. Engel et al., *Ab initio* treatment of collective correlations and the Neutrinoless double beta decay of ^{48}Ca. Phys. Rev. Lett. **124**, 232501 (2020). https://doi.org/10.1103/PhysRevLett.124.232501
42. T. Miyagi, X. Cao, R. Seutin et al., Impact of two-body currents on magnetic dipole moments of nuclei. Phys. Rev. Lett. **132**, 232503 (2024). https://doi.org/10.1103/PhysRevLett.132.232503
43. B. Acharya, B.S. Hu, S. Bacca et al., Magnetic dipole transition in ^{48}Ca. Phys. Rev. Lett. **132**, 232504 (2024). https://doi.org/10.1103/PhysRevLett.132.232504
44. T. Miyagi, Nuhamil: A numerical code to generate nuclear two- and three-body matrix elements from chiral effective field theory. Eur. Phys. J. A **59**, 150 (2023). https://doi.org/10.1140/epja/s10050-023-01039-y